Available online at www.sciencedirect.com

SciVerse ScienceDirect

Ceramics International 39 (2013) 2675–2682

CERAMICS INTERNATIONAL

www.elsevier.com/locate/ceramint

Preparation, structural and luminescent properties of $YAl_3(BO_3)_4$:Dy^{3+} phosphor for white light-emission under UV excitation

G.V. Lokeswara Reddy[a], L. Rama Moorthy[a,b,*], B.C. Jamalaiah[c], T. Sasikala[a]

[a]Department of Physics, Sri Venkateswara University, Tirupati 517502, India
[b]Department of Physics, Chadalawada Ramanamma Engineering College, Renigunta Road, Tirupati 517506, India
[c]Ceramic and Glass Engineering Department, CICECO, University of Aveiro, Campus Santiago, 3810-193 AVEIRO, PORTUGAL

Received 15 August 2012; accepted 12 September 2012
Available online 3 October 2012

Abstract

A series of $YAl_3(BO_3)_4$ phosphors doped with different concentrations of Dy_2O_3 ($0.1 \le x \le 5$ mol%) were prepared by solid-state reaction method. The crystallization process of the precursor has been examined by differential thermal analysis (DTA) measurements. The phase purity and surface morphological features were characterized by X-ray diffraction (XRD) and scanning electron microscopic (SEM) investigations. The $YAl_3(BO_3)_4$ nanocrystals obtained were found to be about 45 nm in size and have the trigonal structure with some agglomeration. Fourier transform infrared (FTIR) and energy dispersive X-ray spectra (EDS) measurements were carried out to understand the compositional and elemental analysis. The characteristics emission peaks of Dy^{3+} ion corresponding to the transitions of $^4F_{9/2} \rightarrow {}^6H_{15/2}$ at 485 nm and $^4F_{9/2} \rightarrow {}^6H_{13/2}$ at 576 nm were observed in the emission spectra. The luminescence quenching noticed at higher Dy_2O_3 concentrations is due to the exchange interaction among the excited Dy^{3+} ions.

Keywords: A. Powder: solid state reaction; C. Lifetime; Luminescence

1. Introduction

White-light emitting diode (w-LED) is considered to be the next generation solid-state light source that will replace the conventional incandescent and fluorescent lamps because of its high luminous efficiency, energy saving and environmental safety [1,2]. The commercial white-light emitting diodes (w-LEDs) are the combination of blue GaN-based LED chip with yellow-emitting YAG:Ce^{3+} phosphor, which shows poor illumination and low color rendering index [3]. In order to develop practically applicable w-LEDs, novel tricolor phosphors are required which can be effectively excited by near ultra violet (nUV) light. Generally, for Dy^{3+} ion the emission color of the luminescence is close to white light because of its yellow (~570–600 nm) and blue (~470–500 nm) emissions. Therefore, it is possible to obtain white light from Dy^{3+} ion activated luminescent materials by adjusting the intensity ratio of yellow to blue emissions by choosing different hosts. The emission of white-light from Dy^{3+}-doped phosphors has been reported in different hosts, such as borates [4], phosphates [5], vanadates [6], molybdates [7] and silicates [8]. Among these, the borate and oxyborate phosphors have attracted more due to their excellent spectral properties, chemical durability and potential applications for different optical devices.

In this study, to obtain an optimal white-light emitting phosphor for different lighting applications, a series of $Y_{(1-x)}Al_3(BO_3)_4$:xDy^{3+} (YAB) phosphors ($0.1 \le x \le 5.0$ mol%) were synthesized by the solid-state reaction method and the luminescent characteristics under nUV excitation were examined. Also, the concentration dependence of luminescence intensities, decay times of $^4F_{9/2}$ excited state and the chromatic properties of Dy^{3+} ions were discussed.

2. Experimental

Different concentrations (0.1–5.0 mol%) of Dy^{3+} ions activated $Y_{(1-x)}Al_3(BO_3)_4$ (YAB) phosphors were prepared by the solid-state reaction method. The starting

*Corresponding author at: Department of Physics, Sri Venkateswara University, Tirupati 517502, India. Tel./fax: +91 877 2289472.
E-mail address: lrmphysics@yahoo.co.in (L. Rama Moorthy).

0272-8842/$ - see front matter © 2012 Elsevier Ltd and Techna Group S.r.l. All rights reserved.
http://dx.doi.org/10.1016/j.ceramint.2012.09.034

materials Al_2O_3 (99.9%), H_3BO_3 (99.9%), Y_2O_3 (99.99%) and Dy_2O_3 (99.99%) were grinded in an agate mortar by adding a small amount of acetone to mix the materials homogeneously (3% excess of H_3BO_3 has been added to compensate the evaporation in heating process). The powder samples were fired at 200 and 600 °C for 3 h in each step with an intermediate grinding. Finally, they were sintered at 1200 °C for 3 h in air using alumina crucible.

The crystallization process of the precursor was examined by differential thermal analysis (DTA) measurements carried out with a TA 5000/SDT 2960 DSC Q 10 under N_2 atmosphere at heating rate of 10 °C/min. The crystalline structure of YAB phosphors was inspected by a X'Pert-Pro Materials Research Diffractometer using CuK_α radiation (λ=1.5406 Å), operating at 40 kV and 30 mA over the range 10–60° (2 Th). The scanning electron microscope-energy dispersive X-ray spectra (SEM-EDS) of undoped and 2.0 mol% Dy^{3+} ions doped YAB phosphors were recorded with an Oxford instruments INCA PENTA FET × 3 attached to SEM: Carl Zeiss EVO MA15. The Fourier transform infrared (FTIR) spectrum was taken with a Thermo Nicolet IR200 spectrophotometer. The excitation, emission and decay measurements were carried out with a Jobin YVON Fluorolog-3 spectrofluorimeter.

3. Results and discussion

3.1. Structural analysis

The DTA curve of YAB precursor in the range 22–1300 °C is shown in Fig. 1. The endothermic peaks observed at 120 and 155 °C are possibly due to the vaporization of physisorbed water and acetone, while the broad exothermic peak might be due to the phase transition of YAB phosphor. The two exothermic (~718 and 926 °C) and one endothermic (~1080 °C) peaks belong to the YBO_3 [9,10]. However, the two exothermic peaks around 1158 and 1220 °C are due to the $YAl_3(BO_3)_4$ phosphor.

Fig. 2 illustrates the XRD patterns of un-doped and 2.0 mol% of Dy^{3+}-doped YAB phosphors along with the standard JCPDS (no. 72-1978) card of YAB phosphor. The XRD patterns of un-doped and different concentrations of Dy^{3+}-doped YAB phosphors sintered at 1200 °C/3 h exhibited the same phase and comparable with the $YErAl_3(BO_3)_4$ powder, prepared by sol–gel technique [11]. It is well known that the structure of the YAB phosphor belongs to the double borates which have the trigonal structure of huntite $CaMg_3(CO_3)_4$ with space group R32. Beregi et al. [12] reported that the formation of YAB phase needs the sintering at temperature range of 1000–1200 °C. Madarasz et al. [10] concluded that considerable amount of YAB has been obtained during the long term (10 h) sintering at 1150 °C. The possible loss of B_2O_3 causes the appearance of intermediate phases. In the present investigation, we succeeded in obtaining the YAB phase with good amount. The intense XRD peaks are in good agreement with the standard JCPDS card of YAB, while the peaks of lower intensity are attributed to the YBO_3 phase (JCPDS no. 74-1929) [10,12]. The presence of small amount of YBO_3 phase could be either due to stoichiometric imbalance (boron loss due to its volatility at higher temperatures) or the slower reaction rate of aluminum oxide with yttrium and boron oxides [11]. The mean crystallite size of the synthesized YAB phosphor has been estimated by Scherrer's equation:

$$D_{hkl} = \frac{0.89\lambda}{\beta_{(2\theta)} Cos\ \theta} \quad (1)$$

where $\beta_{(2\theta)}$ is the full width at half maximum of the pure diffraction profile in radians, λ is the wavelength of the X-rays, θ is the angle of diffraction and D_{hkl} is the average

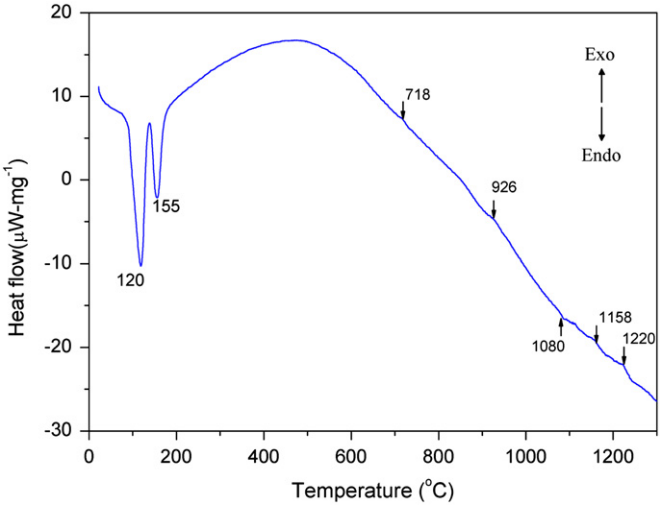

Fig. 1. DTA curve of YAB precursor.

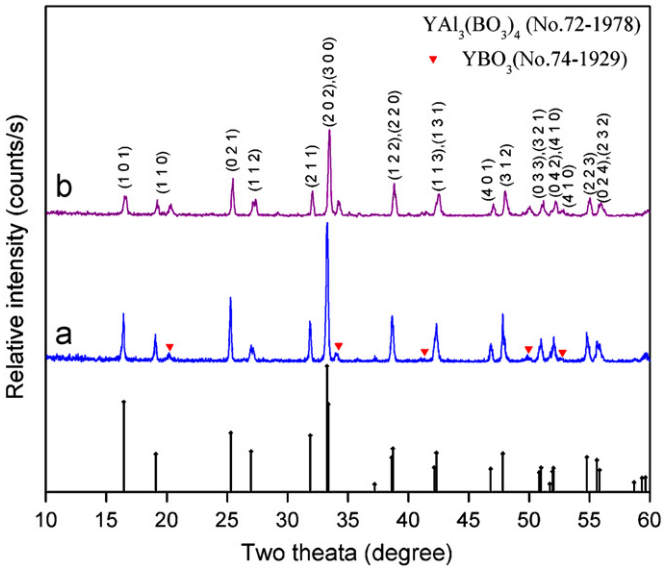

Fig. 2. XRD profiles of: (a) un-doped and (b) 2.0 mol% Dy^{3+}-doped YAB phosphors.

diameter of the crystallite. By substituting XRD data of various peaks to Eq. (1), the average crystallite size for the YAB phosphor is found to be about 45 nm. Observed XRD data and corresponding crystallite sizes are listed in Table 1.

The FTIR spectrum of YAB phosphor sintered at 1200 °C/3 h is shown in Fig. 3. In the borate compounds containing $(BO_3)^{3-}$ groups, the electronic delocalization in planar borate anions is more predominant. From the FTIR spectrum, various B–O arrangements in YAB powder phosphor are implicit. The IR bands located at around 1251 and 1354 cm^{-1} could be due to the B–O bond stretching vibrations of $(BO_3)^{3-}$ units, while the band at ~1413 cm^{-1} is due to asymmetric stretching relaxation of the B–O bond of trigonal units. However, the band at ~500 cm^{-1} could be due to the B–O–B bending vibrations [12]. A group of bands around 461, 541 and 613 cm^{-1} are the characteristics of Y–O stretching vibrations while the bands located at around 706 and 775 cm^{-1} represent the Al–O stretching vibrations [13,14]. The IR absorption bands around 868, 917 and 1064 cm^{-1} are due to the YBO_3 impurified phase [11,15]. In order to confirm the formation of YAB phase using the Y_2O_3 (99.99%), Al_2O_3 (99.9%) and H_3BO_3 (99.9%) as starting chemicals, it requires further investigation with various heat treatment time durations and temperatures in the range 1000–2000 °C by the solid state reaction technique.

Table 1
Powder XRD data and the corresponding crystallite size of YAB phosphor.

XRD peak position 2θ (°)	Relative intensity (%)	$\beta_{(2\theta)}$ 2θ (°)	D_{hkl} (nm)
16.6101	21.05	0.1181	67.26
19.1682	14.92	0.1968	40.51
25.4282	42.72	0.0984	81.88
27.0782	14.32	0.1181	68.46
32.0243	18.65	0.1181	69.24
33.4244	100.00	0.2165	37.90
38.7872	34.82	0.1968	42.34
42.4919	24.51	0.1968	42.85
47.0185	12.75	0.2362	36.29
47.9872	28.72	0.2362	36.42
51.1013	13.29	0.3149	27.67
52.1815	15.32	0.1968	44.47
54.9848	18.51	0.3149	28.14
55.8852	13.01	0.4723	18.84

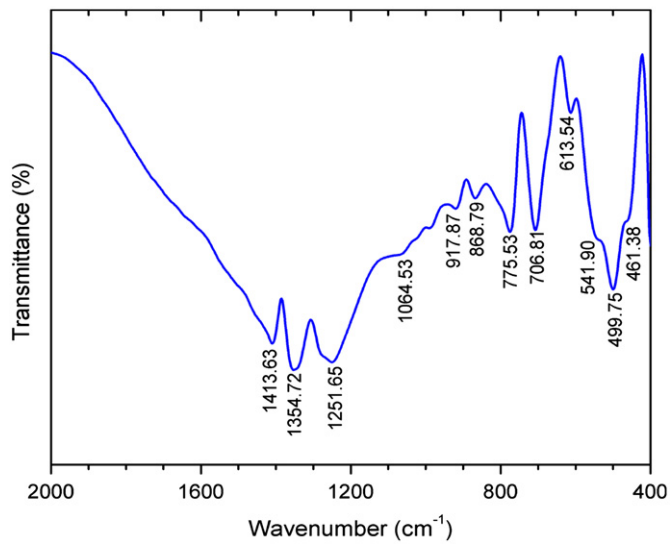

Fig. 3. FTIR spectrum of the YAB phosphor heat treated at 1200 °C.

The chemical composition of un-doped and 2.0 mol% Dy^{3+}-doped YAB phosphors has been confirmed by recording the EDS spectra as illustrated in Fig. 4(a) and (b) respectively. The spectral data of un-doped YAB phosphor provide 65.12 atm% of oxygen. Apart from oxygen, all the other elements that include boron (18.57 atm%), aluminum (11.36 atm%) and yttrium (4.95 atm%) are given separately confirming their presence (see Fig. 4(a)). The details of the elements present in 2.0 mol% Dy^{3+}-doped YAB are listed in Fig. 4(b). It is well known that the phosphor with regular morphology and fine grain size is more useful for the enhancement of luminescence performance in the device fabrication [16]. Furthermore, the morphology of resultant phosphor usually depends on the morphology of the starting materials, the sintering temperature, reaction duration and the amount of flux. Fig. 4(c) and (d) represents the SEM images of un-doped and 2.0 mol% Dy^{3+}-doped YAB phosphors, respectively. It can be seen that the images exhibits trigonal structure with micro-meter sized particles due to the amalgamation. Thus, it is suggested that the morphology of the studied phosphors must be improved in order to meet the practical device applications.

3.2. Excitation spectrum

The excitation spectrum in the spectral range 300–500 nm recorded for 2.0 mol% Dy^{3+}-doped YAB phosphor monitoring the emission at 576 nm is shown in Fig. 5. The spectrum displayed a total of eight bands centered at 326, 338, 352, 367, 387, 426, 453 and 475 nm corresponding to the intrinsic f–f transitions of Dy^{3+} ion from the ground state $^6H_{15/2}$ to the excited states $^6P_{3/2}$, $^4I_{9/2}$, $^6P_{7/2}$, $^6P_{5/2}$, $^4F_{7/2}$, $^4G_{11/2}$, $^4I_{15/2}$ and $^4F_{9/2}$ respectively. The intense peaks observed at 352 and 387 nm indicate that the near-UV and blue LEDs can be used as pumping sources to obtain efficient emission in the case of Dy^{3+} ions. Furthermore, the intensity of peaks increases with the increase of Dy^{3+} ion concentration and reaches a maximum for 2.0 mol% and then decreases as shown in inset of Fig. 5. This may be due to the self-quenching of excited Dy^{3+} ions, when the concentration of Dy^{3+} is more than 2.0 mol%.

3.3. Emission spectra

In the present investigation, the emission spectra of YAB:xDy^{3+} ($0.1 \le x \le 5$ mol%) phosphors recorded in

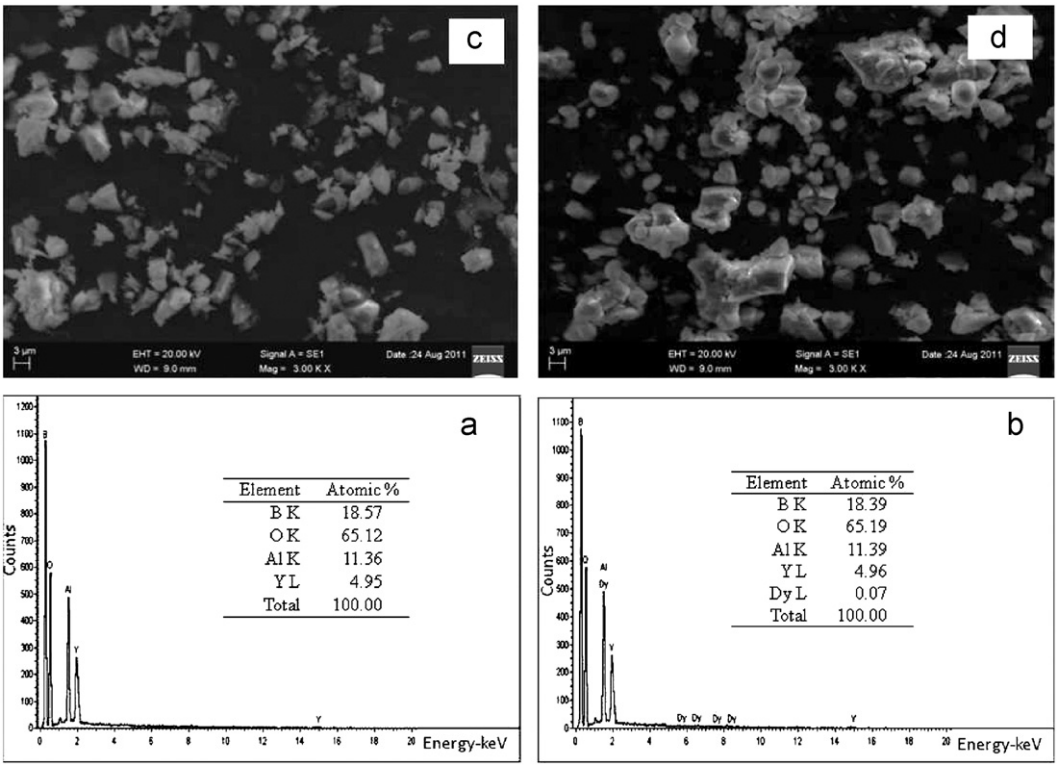

Fig. 4. The EDS spectra of: (a) un-doped and (b) 2% Dy^{3+}-doped YAB phosphors, (c) and (d) show corresponding SEM images.

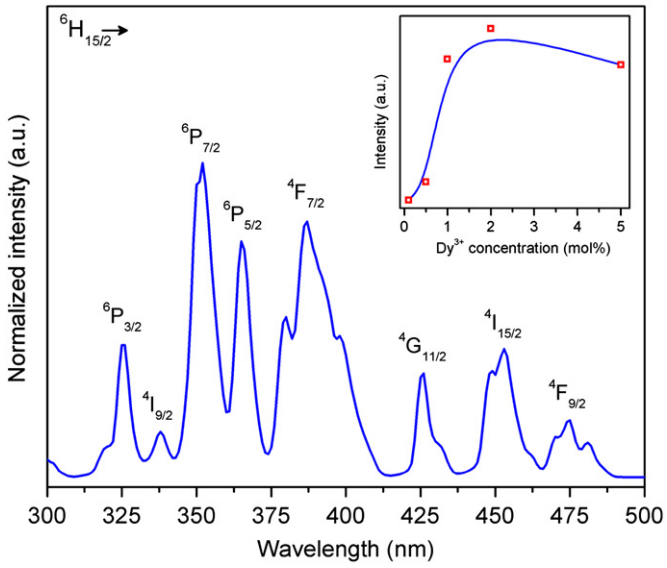

Fig. 5. Excitation spectrum (λ_{em}=576 nm) of 2.0 mol% of Dy^{3+}-doped YAB phosphor. Inset show the intensity variation of $^6H_{15/2}\rightarrow{}^6P_{7/2}$ (352 nm) transition as a function of Dy^{3+} ion concentrations.

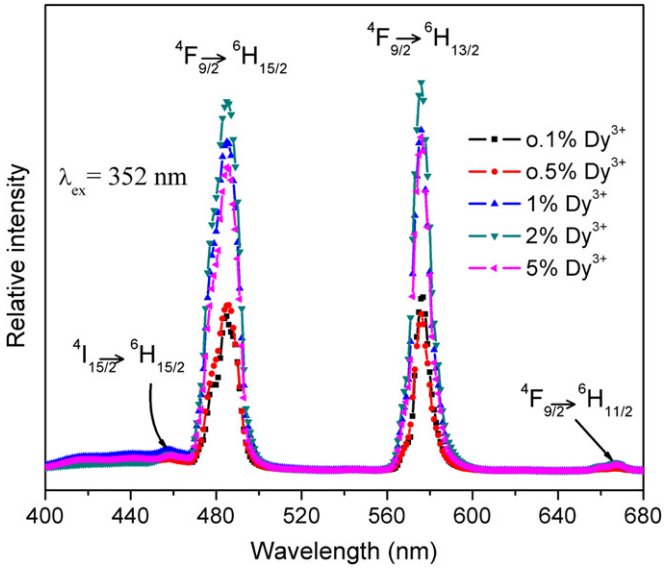

Fig. 6. Luminescence spectra of different concentrations of Dy^{3+}-doped YAB phosphors under 352 nm excitation.

the spectral range 400–680 nm by exciting at 352 nm wavelength are shown in Fig. 6. The intense emission bands observed at 486 nm (blue), 576 nm (yellow) and a feeble band at 666 nm (red) are assigned to $^4F_{9/2}\rightarrow{}^6H_{15/2}$, $^4F_{9/2}\rightarrow{}^6H_{13/2}$ and $^4F_{9/2}\rightarrow{}^6H_{11/2}$ transitions of Dy^{3+} ion respectively. In addition to these emission bands, a weak band noticed at about 458 nm is attributed to the $^4I_{15/2}\rightarrow{}^6H_{15/2}$ transition. The emission channels of Dy^{3+} ion in YAB phosphors are given in a partial energy level diagram shown in Fig. 7.

To investigate the effect of excitation wavelength on luminescence, the visible emission spectra of 2.0 mol% Dy^{3+}-doped YAB phosphors recorded with different excitation wavelengths are depicted in Fig. 8. The inset of Fig. 8 shows the variation of emission intensity of $^4F_{9/2}\rightarrow{}^6H_{15/2}$ and $^4F_{9/2}\rightarrow{}^6H_{13/2}$ transitions with different

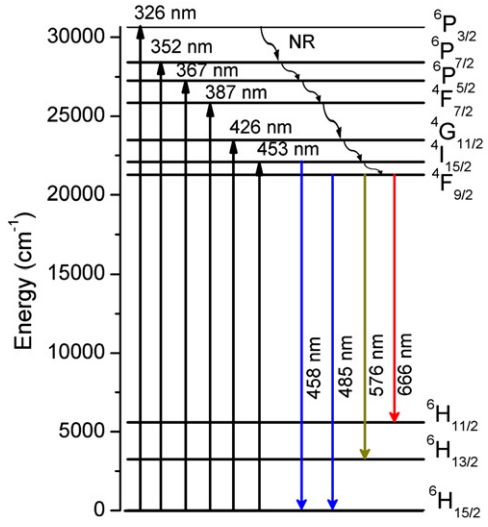

Fig. 7. Energy level diagram showing the emissions of Dy^{3+} ion in YAB phosphor at different excitation wavelengths.

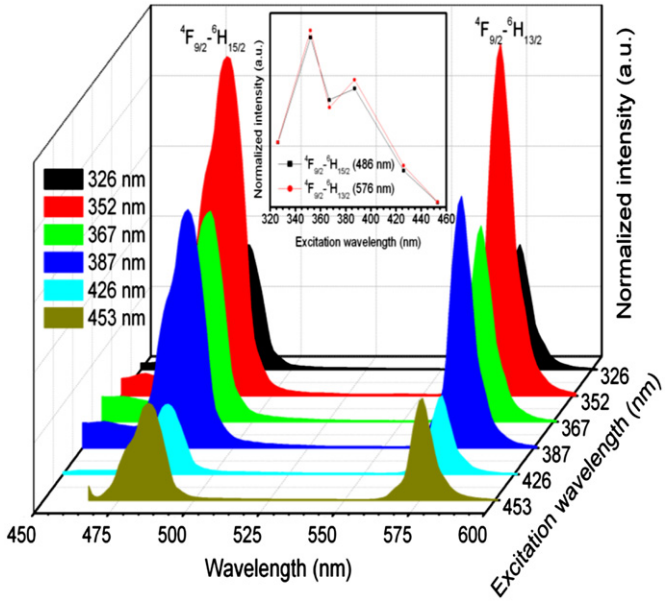

Fig. 8. Luminescence spectra of 2.0 mol% Dy^{3+}-doped YAB phosphor at different excitation wavelengths. Inset is the intensity variation of $^4F_{9/2} \rightarrow {}^6H_{15/2,13/2}$ transitions as a function of excitation wavelengths.

excitation wavelengths. From these results, it is evident that YAB phosphor containing 2.0 mol% of Dy^{3+} ions exhibits efficient luminescence under 352 and 387 nm excitation wavelengths. It is also well known that the $^4F_{9/2} \rightarrow {}^6H_{15/2}$ (blue) transition hardly varies with the environment, while the $^4F_{9/2} \rightarrow {}^6H_{13/2}$ (yellow) is the hypersensitive transition, which is strongly influenced by the ligand environment. The relative intensities of these two emission band depend strongly on the local symmetry of Dy^{3+} ions. Normally the lower symmetry local site results in the higher yellow to blue luminescence (Y/B) intensity ratio. The Y/B ratios determined for YAB:$x$$Dy^{3+}$ phosphors are presented in Table 2. For the present phosphor materials (under 352 nm excitation), the Y/B ratios are found to be almost unity.

Table 2
The yellow to blue ratios (Y/B) of YAB:$x$$Dy^{3+}$ phosphors at different concentrations (λ_{ex}=352 nm) and also at different excitation wavelengths for x=2.0 mol% of Dy^{3+} ions.

Concentration, x (%)	Y/B	x=2.0 mol%	
		Excitation wavelengths (nm)	Y/B
0.1	1.0078	326	1.0046
0.5	0.9462	352	1.0580
1.0	1.0424	367	0.9289
2.0	1.0580	387	1.0770
5.0	1.1078	426	1.1539
		453	1.3360

Similarly, the Y/B ratio is also nearly unity for 2.0 mol% of Dy^{3+}-doped YAB phosphor excited with different wavelengths. These results revealed that the Dy^{3+} ions are located at lower symmetry sites in YAB phosphor.

3.4. Effect of Dy^{3+} concentration and energy transfer mechanism

To optimize the dopant concentration for efficient luminescence, the concentration of Dy^{3+} ions in YAB phosphor has been varied from 0.1 to 5.0 mol%. Upon 352 nm excitation, the luminescence intensities of the YAB:$x$$Dy^{3+}$ ($0.1 \le x \le 5.0$ mol%) phosphors increases with the increase of Dy^{3+} ion concentration, reaches a maximum value for 2.0 mol% of Dy^{3+} and then decreases for further increase of concentration due to energy transfer among the excited Dy^{3+} ions at higher concentrations. The intensity variation of blue ($^4F_{9/2} \rightarrow {}^6H_{15/2}$) and yellow ($^4F_{9/2} \rightarrow {}^6H_{13/2}$) emissions with Dy^{3+} ions concentration is illustrated in Fig. 9(a). From this figure, it is clear that the luminescence intensity is maximum for x=2.0 mol%. Normally, the distance between the Dy^{3+} luminescent ions decreases with the increase of Dy^{3+} ion concentration and hence, energy transfer among the Dy^{3+} ions increases. The critical distance (R_c) between the nearest Dy^{3+} ions at which energy transfer occurs is given by [17]:

$$R_c = 2\left(\frac{3V}{4\pi x_c N}\right)^{1/3} \quad (2)$$

where V is the volume of the unit cell, x_c is the critical concentration of Dy^{3+} ions and N is the number of available crystallographic sites occupied by Dy^{3+} ions in unit cell. The values of V, x_c and N are 541.94 Å, 0.02 and 3, respectively. For YAB:$x$$Dy^{3+}$ ($0.1 \le x \le 5$ mol%) phosphors, the value of R_c is determined as 25.84 Å, which is close to the $NaCaPO_4$:Dy^{3+} phosphor [18].

The energy transfer is generally associated with multipolar interactions, radiation re-absorption or exchange interaction. These effects can be identified by examining the intensities of emission bands obtained by direct measurement under equilibrium conditions as a function of the

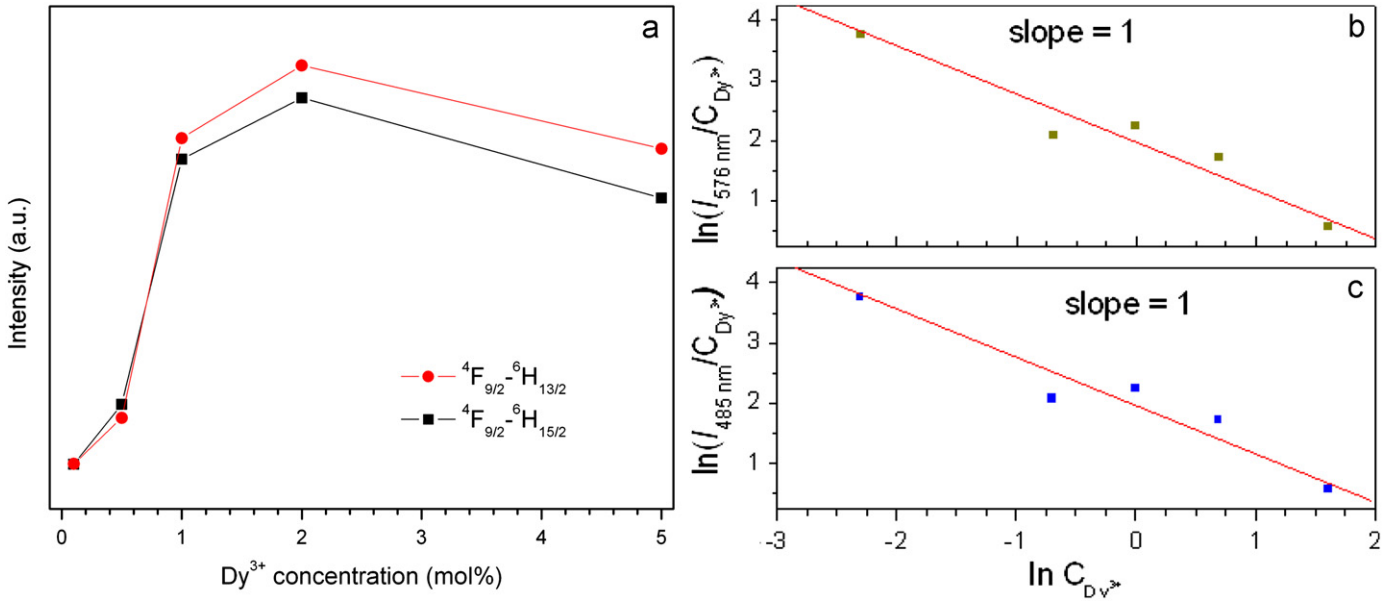

Fig. 9. (a) Variation of intensity of $^4F_{9/2} \rightarrow {}^6H_{15/2,13/2}$ transitions as a function of Dy^{3+} concentration, (b) and (c) are the logarithmic plots for the luminescence intensity per activator ion as a function of the activator concentration at 576 nm and 485 nm respectively.

excited and/or ion concentration. Among these, the multipolar interactions such as dipole–dipole (*d–d*), dipole–quadrupole (*d–q*) and quadrupole–quadrupole (*q–q*) are usually prevalent. When direct multipolar interactions are involved, quenching is generally more extensive. However, the exchange interaction is limited to nearest or next nearest neighbor between the rare earth ions. If the migration is rapid compared to direct transfer, the quenching tends to be proportional to activator ions concentration. For a better understanding of energy transfer mechanism, the relationship between the emission intensity and activator concentration has been considered. The type of energy transfer from the emitting level can be determined from the change in the emission intensity [19]. The emission intensity (I) per activator ion is given as

$$\frac{I}{C_A} = \frac{1}{K[1+\beta C_A{}^{S/3}]} \tag{3}$$

where C_A is the activator concentration, I/C_A is the emission intensity (I) per activator concentration. The factors K and β are constants for the particular excitation condition of given host material. The values of S are 3, 6, 8 and 10 for exchange, dipole–dipole (*d–d*), dipole–quadrupole (*d–q*) and quadrupole–quadrupole (*q–q*) interactions, respectively. The above equation can simply be rearranged as follows [20]:

$$\ln\left(\frac{I}{C_A}\right) = K' - \frac{S}{3}\ln C_A \tag{4}$$

where $K' = [\ln K - \ln\beta]$. The concentration dependent curves of $ln(I/C_A)$- versus $ln\ C_A$ for yellow (576 nm) and blue (485 nm) emissions are plotted as shown in Fig. 9(b) and (c), respectively. From the slopes of these curves (slope= $S/3=1$), the value of S obtained are approximately equal to 3, which means that the quenching is directly proportional to the ion concentration. These results indicate that the concentration quenching in the present case is caused by the exchange interaction among the Dy^{3+} ions.

3.5. Color perception

In order to evaluate the colorimetric performance of phosphors, the color coordinates are determined using the intensity calibrated emission spectral data and the chromatic standard issued by the Commission International de I'Eclairage in 1931 (CIE-1931). The evaluated CIE coordinates for the Dy^{3+}-doped YAB phosphors located graphically in Fig. 10(a) are presented in Table 3. As can be seen from Fig. 10(a), the samples containing ≥ 1.0 mol% of Dy^{3+} ions exhibit potential white light under 352 nm UV excitation, when the excitation wavelengths changes from UV to n-UV to Vis, the emitting color changes in the order reddish-yellow to white to greenish-yellow as illustrated in Fig. 10(b). However, they emit pure white light under n-UV excitation. The calculated CIE coordinates for 2.0 mol% of Dy^{3+}-doped YAB phosphor are $x=0.3113$ and $y=0.3303$, and comparable to 2.0 mol% Dy^{3+}-doped YVO_4 ($x=0.3601$, $y=0.3715$ and $\lambda_{ex}=223$ nm) [21], $LaPO_4$ ($x=0.312$, $y=0.318$ and $\lambda_{ex}=147$ nm) [22], $Ca_2Gd_8(SiO_4)_6O_2$ ($x=0.353$, $y=0.382$ and $\lambda_{ex}=172$ nm) [23] and $Gd_2(MoO_4)_3$ ($x=0.37$, $y=0.38$ and $\lambda_{ex}=389$ nm) [24] phosphors. Thus, the YAB phosphors with 2.0 mol% of Dy^{3+} concentration are highly useful for white-light emission under 352 nm UV excitation.

3.6. Decay analysis

The decay profiles of $^4F_{9/2}$ emission level for different concentrations of Dy^{3+} ion in YAB phosphors under 352 nm excitation and by monitoring the emission at

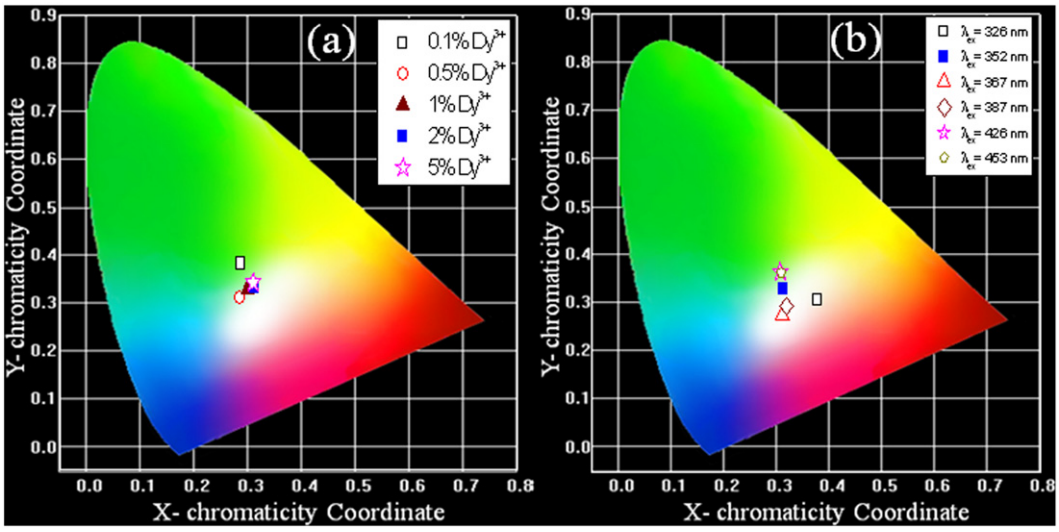

Fig. 10. Location of chromaticity coordinates for Dy^{3+}-doped YAB phosphors: (a) for different Dy^{3+} concentrations under 352 nm UV excitation and (b) for 2.0 mol% Dy^{3+} ions under different excitation wavelengths.

Table 3
Chromaticity coordinates of YAB:xDy^{3+} phosphors at different concentrations (λ_{ex}=352 nm) and at different excitation wavelengths for x=2.0 mol%.

Concentration of Dy^{3+}, x (%)	x-coordinate	y-coordinate	Excitation wavelengths (nm)	x=2.0 of Dy^{3+} ions	
				x-coordinate	y-coordinate
0.1	0.2853	0.3808	326	0.3783	0.3065
0.5	0.2838	0.3101	352	0.3113	0.3303
1.0	0.2976	0.3277	367	0.3106	0.2750
2.0	0.3113	0.3303	387	0.3182	0.2939
5.0	0.3083	0.3411	426	0.3068	0.3649
			453	0.3083	0.3634

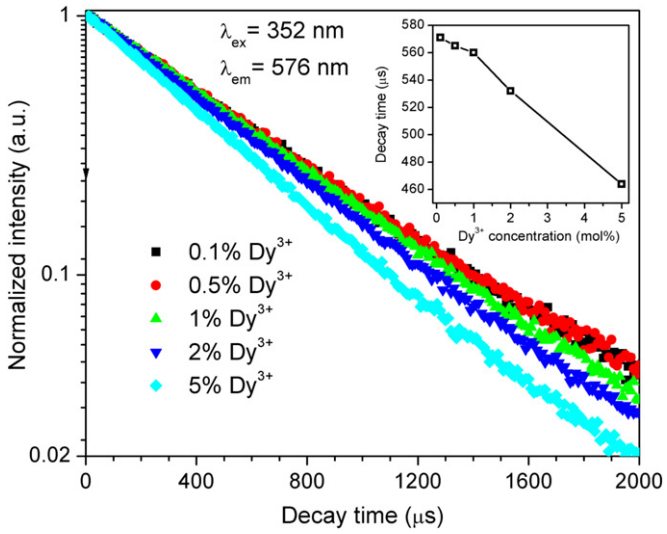

Fig. 11. Logarithmic plot of decay profiles of different concentrations of Dy^{3+} -doped YAB phosphors under 352 nm excitation. Inset shows the variation of decay time as a function of Dy^{3+} ions concentration.

576 nm are illustrated in Fig. 11. The decay profiles are found to be single exponential for all the concentrations. However, the decay times decreases with the increase of Dy^{3+} ion concentration from 0.1 to 5.0 mol%. The quenching in decay time with Dy^{3+} ion concentration may be due to the exchange interaction among the excited Dy^{3+}–Dy^{3+} ions. The decay times measured by taking the first e-folding times of the luminescence intensity are 571, 565, 560, 532 and 464 μs for 0.1, 0.5, 1.0, 2.0 and 5.0 mol% Dy^{3+} ion concentrations, respectively. From these values it is concluded that the Dy^{3+}-doped YAB phosphors exhibit longer decay times than those of the previously reported phosphor materials [25–27].

4. Conclusions

Structural and luminescent properties of an efficient white light-emitting $Y_{(1-x)}Al_3(BO_3)_4:Dy^{3+}_x$ ($0.1 \leq x \geq 5.0$ mol%) YAB phosphors were prepared by solid-state reaction method. The structure, morphology and compositional details have been examined using XRD, FESEM, EDS and FTIR measurements. The estimated average crystallite size of the YAB:Dy^{3+} phosphor is about 45 nm. The excitation and emission spectra revealed that the YAB:Dy^{3+} phosphors emit intense white light under the excitation of 352 and 387 nm n-UV light. The effect of concentration quenching mechanism on the $^4F_{9/2} \rightarrow {}^6H_{13/2}$

(yellow) and $^4F_{9/2} \rightarrow {}^6H_{15/2}$ (blue) transitions of Dy^{3+} ions in YAB phosphor has been attributed to the exchange interaction among the excited Dy^{3+} ions at higher concentrations. The chromaticity coordinates for 2.0 mol% Dy^{3+}-doped YAB phosphor are $x=0.3113$ and $y=0.3303$. The experimental results confirmed that the YAB phosphor containing 2.0 mol% of Dy^{3+} ions is more useful for white-lighting applications under n-UV excitation.

Acknowledgment

One of the authors Prof. L. Rama Moorhy would like to thank the Council of Scientific and Industrial Research (CSIR), New Delhi, India for sanction of financial support in the form of major research projects no. 03(1224)/12/EMR-II.

References

[1] Y. Chen, K.W. Cheah, M. Gong, Low thermal quenching and high-efficiency Ce^{3+}, Tb^{3+}-codoped $Ca_3Sc_2Si_3O_{12}$ green phosphor for white-light emitting diodes, Journal of Luminescence 131 (2011) 1589–1593.

[2] N. Yeh, J.P. Chung, High-brightness LEDs-Energy efficient lighting sources and their potential in indoor plant cultivation, Renewable and Sustainable Energy Reviews 13 (2009) 2175–2180.

[3] S. Neeraj, N. Kijima, A.K. Cheetham, Novel red phosphors for solid-state lighting: the system $NaM(WO_4)_{2-x}(MoO_4)x:Eu^{3+}$ (M=Gd, Y, Bi), Chemical Physics Letters 387 (2004) 2–6.

[4] Y. Liu, Z. Yang, Q. Yu, X. Li, Y. Yang, P. Li, Luminescence properties of $Ba_2LiB_5O_{10}:Dy^{3+}$ phosphor, Materials Letters 65 (2011) 1956–1958.

[5] K.N. Shinde, S.J. Dhoble, A. Kumar, Synthesis of novel Dy^{3+} activated phosphate phosphors for NUV excited LED, Journal of Luminescence 131 (2011) 931–937.

[6] D.C. Yu, S. Ye, M.Y. Peng, Q.Y. Zhang, J.R. Qiu, J. Wang, L. Wondraczek, Efficient near-infrared downconversion in $GdVO_4:Dy^{3+}$ phosphors for enhancing the photo-response of solar cells, Solar Energy Materials and Solar Cells 95 (2011) 1590–1593.

[7] Y. Tian, B. Chen, B. Tian, R. Hua, J. Sun, L. Cheng, H. Zhong, X. Li, J. Zhang, Y. Zheng, T. Yu, L. Huang, Q. Meng, Concentration-dependent luminescence and energy transfer of flower-like $Y_2(MoO_4)_3:Dy^{3+}$ phosphor, Journal of Alloys and Compounds 509 (2011) 6096–6101.

[8] R.P. Wei, Z.H. Jua, J.X. Ma, D. Zhang, Z.P. Zang, W.S. Liu, A novel white afterglow phosphorescent phosphor $Ca_3SnSi_2O_9:Dy^{3+}$, Journal of Alloys and Compounds 486 (2009) L17–L20.

[9] S. Sweeney, Thermochemical studies of group IIIB borates and mixed borates, Thermochimica Acta 11 (1975) 397–407.

[10] J. Madarasz, E. Beregi, J. Sztatisz, I. Földvari, G. Pokol, Combined DTA and XRD study of sintering steps towards $YAl_3(BO_3)_4$, Journal of Thermal Analysis and Calorimetry 64 (2001) 1059–1065.

[11] L.J.Q. Maia, A. Ibanez, L. Ortega, V.R. Mastelaro, A.C. Hernandes, Er:YAB nanoparticles and vitreous thin films by the polymeric precursor method, Journal of Nanoparticle Research 10 (2008) 1251–1262.

[12] E. Beregi, A. Watterich, L. Kovacs, J. Madarasz, Solid-state reactions in Y_2O_3:$3Al_2O_3$:$4B_2O_3$ system studied by FTIR spectroscopy and X-ray diffraction, Vibrational Spectroscopy 22 (2000) 169–173.

[13] B. Yan, C. Wang, Synthesis and luminescence properties of $REAl_3(BO_3)_4:Eu^{3+}/Tb^{3+}$ (RE=Y, Gd) phosphors from sol–gel composition of hybrid precursors, Solid State Sciences 10 (2008) 82–89.

[14] P. Apte, H. Burke, H. Pickup, Synthesis of yttrium aluminum garnet by reverse strike precipitation, Journal of Materials Research 7 (1992) 706–711.

[15] Z. Xu, J. Yang, Z. Hou, C. Li, C. Zhang, S. Huang, J. Lin, Hydrothermal synthesis and luminescent properties of $Y_2O_3:Tb^{3+}$ microrods, Materials Research Bulletin 44 (2009) 1850–1857.

[16] Y.C. Kang, M.A. Lim, H.D. Park, M. Han, Ba^{2+} co-doped Zn_2SiO_4:Mn phosphor particles prepared by spray pyrolysis process, Journal of the Electrochemical Society 150 (2003) H7–H11.

[17] G. Blasse, Energy transfer in oxide phosphors, Philips Research Reports 24 (1969) 131–144.

[18] B.V. Ratnam, M. Jayasimhadri, Kiwan Jang, Ho Sueb Lee, Soung-Soo Yi, Jung-Hyun Jeong, White light emission from $NaCaPO_4$: Dy31 phosphor for ultraviolet-based white light-emitting diodes, Journal of the American Ceramic Society 93 (2010) 3857–3861.

[19] I.G. Van Uitert, Characterization of energy transfer interactions between rare earth ions, Journal of the Electrochemical Society 114 (1967) 1048–1053.

[20] H.Y. Du, J.F. Sun, Z.G. Xia, J.Y. Sun, Luminescence properties of $Ba_2Mg(BO_3)_2:Eu^{2+}$ red phosphors synthesized by a microwave-assisted sol–gel route, Journal of the Electrochemical Society 156 (2009) J361–J366.

[21] S.D. Han, S.P. Khatkar, V.B. Taxak, G. Sharma, D. Kumar, Synthesis, luminescence and effect of heat treatment on the properties of Dy^{3+}-doped YVO_4 phosphor, Materials Science and Engineering B 129 (2006) 126–130.

[22] G. Han, Y. Wang, C. Wu, J. Zhang, Hydrothermal synthesis and vacuum ultraviolet-excited luminescence properties of novel Dy^{3+}-doped $LaPO_4$ white light phosphors, Materials Research Bulletin 44 (2009) 2255–2257.

[23] Y. Wang, Y. Wen, F. Zhang, Novel Dy^{3+}-doped $Ca_2Gd_8(SiO_4)_6O_2$ white light phosphors for Hg-free lamps application, Materials Research Bulletin 45 (2010) 1614–1617.

[24] X. Yanna, X. Fen, Z. Qinyuan, J. Zhonghong, Synthesis and luminescent properties of polycrystalline $Gd_2(MoO_4)_3:Dy^{3+}$ for white-emitting diodes, Journal of Rare Earths 27 (2009) 753–757.

[25] X. Zhang, H.J. Seo, Luminescence properties of novel Sm^{3+}, Dy^{3+} doped $LaMoBO_6$ phosphors, Journal of Alloys and Compounds 509 (2011) 2007–2010.

[26] G.S.R. Raju, J.Y. Park, H.C. Jung, B.K. Moon, J.H. Jeong, J.H. Kim, Luminescence properties of $Dy^{3+}:GdAlO_3$ nanopowder phosphors, Current Applied Physics 9 (2009) e92–e95.

[27] H. Xiumei, L. Jun, L. Zhe, Q. Xiwei, L. Mingya, W. Xiaoqiang, Photoluminescent properties of $Ca_2Gd_8(SiO_4)_6O_2$: Dy^{3+} phosphor films prepared by sol–gel process, Journal of Rare Earths 26 (2008) 904–906.